Computational Methods for Maximum Drawdown Options Under Jump-Diffusion

by

David Erik Fagnan

A thesis
presented to the University of Waterloo
in fulfilment of the
thesis requirement for the degree of
Master of Mathematics
in
Computer Science

Waterloo, Ontario, Canada, 2011

©David Erik Fagnan 2011

AUTHOR'S DECLARATION

I hereby declare that I am the sole author of this thesis. This is a true copy of the thesis, including any required final revisions, as accepted by my examiners.

I understand that my thesis may be made electronically available to the public.

David Erik Fagnan

Abstract

Recently, the maximum drawdown (MD) has been proposed as an alternative risk measure ideal for capturing downside risk. Furthermore, the maximum drawdown is associated with a Pain ratio and therefore may be a desirable insurance product. This thesis focuses on the pricing of the discrete maximum drawdown option under jump-diffusion by solving the associated partial integro differential equation (PIDE). To achieve this, a finite difference method is used to solve a set of one-dimensional PIDEs and appropriate observation conditions are applied at a set of observation dates. We handle arbitrary strikes on the option for both the absolute and relative maximum drawdown and then show that a similarity reduction is possible for the absolute maximum drawdown with zero strike, and for the relative maximum drawdown with arbitrary strike. We present numerical tests of validation and convergence for various grid types and interpolation methods. These results are in agreement with previous results for the maximum drawdown and indicate that scaled grids using a tri-linear interpolation achieves the best rate of convergence. A comparison with mutual fund fees is performed to illustrate a possible rationalization for why investors continue to purchase such funds, with high management fees.

Acknowledgements

First and foremost, I would like to thank my supervisor, Peter Forsyth for his support and direction during my time at the University of Waterloo. His passion for computational finance drew me in and kept me excited about my research. I am very thankful for his patience during the many rounds of revisions during the writing process and I enjoyed our many discussions and appreciated his ability to schedule our meetings on short notice. In addition, I would like to thank my co-supervisor George Labahn, for his hours spent reading my work and his helpful comments. Finally, I thank my readers for their opinions and insights and for dedicating their time.

Table of Contents

List of Tables

List of Figures

Chapter 1

Introduction

1.1 Overview

Recently, the maximum drawdown (*MD*) has been proposed as an alternative risk measure ideal for capturing downside risk [2, 3]. In fact, it is often compared with the Sharpe ratio as one of the top performance measures, and is widely used in practice [4, 5, 6]. The most popular drawdown-based measure is the Calmar ratio [6], but others include the Pain ratio [7], Ulcer index [7] and Sterling ratio.

Although drawdown measures are widely used, there is a significant gap between practice and theory [6]. Recent work by Schuhmacher *et al.* [6] attempts to bridge this gap by providing theoretical insights into drawdown based measures. Nevertheless, the maximum drawdown is insufficient when it comes to forecasting future drawdowns or performance [5].

On the other hand, it is clear that large drawdowns are something that all investors want to avoid. Loss aversion in behavioural finance suggests that investors feel losses much more than they feel gains [8, 2, 9]. Furthermore, the maximum drawdown is associated with both the Pain ratio and the Ulcer index which both indicate an association between the maximum drawdown and suffering by the investor. A recent article [10] captures this association and develops the idea of the drawdown being an indicator of pain.

In this thesis, we suggest that a maximum drawdown option can provide portfolio protection by providing insurance against large drawdowns. Suppose an investor invests in a risky asset but wants to be protected against large drawdowns in a given time period. The investor can, in addition, purchase a maximum drawdown option on the underlying asset with strike K, which pays out in cases of large drawdowns.

Paying such a premium can be compared to paying mutual fund fees. Since it has been shown that higher mutual fund fees are correlated with lower before-

fee returns, the motivation behind why investors continue to purchase such funds is a topic of debate [11, 12]. One suggestion is that such fees are set strategically, in order to extract surplus from unsophisticated investors [13, 12]. Another explanation is that investors are paying for a service they value, which is unrelated to performance [14]. Following these ideas, investors may believe that the fund manager can prevent large drawdowns, and they may view the fee akin to drawdown insurance.

1.2 Previous Work

The maximum drawdown has been previously studied in literature. Magdon-Ismail first developed analytic expressions for the expected maximum drawdown under Brownian motion [4]. Unfortunately, such analytic solutions have not been extended to the case of Geometric Brownian motion (GBM). More recently, Pospisil and Vecer [15, 16] develop partial-differential equation methods for pricing a forward on the maximum drawdown under GBM [15]. However, a major issue in pricing drawdown claims is the ability to model jumps. Jumps in risky assets are observed in practice and cannot be explained by GBM. Since the maximum drawdown is path-dependent and measures the largest drop over a given period, it is evident that jumps are crucial to an appropriate pricing methodology. Recently, Pospisil and Vecer have extended their model to include jump-diffusion under the special case of a crash option on the maximum relative drawdown (*MRD*) [17].

This thesis extends the model of Pospisil and Vecer to handle jump-diffusion and discrete observations of path-dependent variables for both the *MD* and *MRD*. Following the work of Windcliff *et al.* [18] we solve a set of one dimensional PDEs embedded in a higher-dimensional space. On each discrete observation date, each one dimensional PDE is connected through no-arbitrage observation conditions. This style of approach has been used successfully for several other path-dependent options including Parisian options [19], Asian options [20], shout options [21], cliquet options [18] and many others.

1.3 Main Contributions

Our approach will handle not only the absolute maximum drawdown, but also the relative maximum drawdown which may be more intuitive to investors. We handle the case of an arbitrary strike on the option, which can allow investors protection against larger drawdowns at reduced cost. In many cases the associated three-dimensional problem can be reduced to a two-dimensional problem

via a similarity reduction.

The main contributions in this thesis are

- We value maximum drawdown options under geometric Brownian motion with jump-diffusion by following the work of Pospisil and Vecer.
- We develop a discrete observation approach consistent with path-dependent options in practice.
- We handle arbitrary strikes on the option for both absolute maximum drawdown and relative maximum drawdown. We demonstrate the effectiveness of a strike in reducing the cost of insurance against large drawdowns.
- Although the use of an arbitrary strike would normally result in a 3-D problem, we show that the case of the maximum relative drawdown can be reduced to a 2-D problem via a similarity reduction.

In addition, we validate our work by comparing to the previous work of Vecer [15], as well as Monte Carlo simulations. We compare results with and without jump-diffusion to demonstrate the significant impact of jumps on the option values.

1.4 Outline

Chapter 2 of this thesis outlines the basic financial models of the stock market. It is intended to be targeted at readers with a basic understanding of stochastic differential equations and assumes no knowledge of finance. Along with fundamental models, it presents the financial products of interest including the maximum drawdown and maximum relative drawdown.

Chapter 3 continues the background by using the principle of no arbitrage to set a fair price on financial products. It begins by presenting the Black-Scholes equation and offers some discussion over other valuation methods such as Monte Carlo simulation. Chapter 4 presents the formalism of discrete observation conditions which allow for path-dependent options which form the core focus of this thesis.

Chapter 5 discusses the general boundary and terminal conditions for financial PIDE valuation. In particular, it presents specific examples for the case of the maximum drawdown and maximum relative drawdown option. Following this, Chapter 6 then defines a general similarity reduction and with specific focus on path-dependent financial options.

This thesis is focused primarily on the numerical aspect of the PIDE pricing problem and Chapter 7 discusses all aspects of the numerical solution. Beginning with the basic localization of the problem, it continues on to a specific discretization method to solve the problem. It also provides an overview of the requirements for convergence both with and without a similarity reduction. Finally, it provides some discussion of numerical grid and observation condition interpolation techniques.

Chapters 8 and 9 show the numerical results that demonstrate our algorithm for the maximum drawdown and maximum relative drawdown. In addition to a numerical characterization of grid type and interpolation method, they also provide a validation of our work by comparison with the previous work of Pospisil and Vecer in [15] as well as Monte Carlo simulation. Chapter 9 also provides a possible rationalization for why investors still purchase mutual funds with high management fees. This thesis then draws to a close with Chapter 10, which presents concluding remarks and possible future directions.

Chapter 2

Financial Products and Models

The financial world is focused around selling products with an uncertain payoff at a future point in time. This chapter will describe some of these products and mathematical models that will allow us to set a price on them. When selling such products it is important to establish a fair price, and also to protect yourself from the associated risk. Investment banks typically charge slightly above the fair price and hedge their risk making a slight profit.

2.1 Stocks and Options

The stock market is the simplest form of financial products from which many more complicated products known as derivatives can be created. Investors can purchase shares or stock of a publicly traded company which then evolves over time. Popular stocks are often combined into indices which comprise of many stocks from a range of sectors and attempt to reflect the economy. Figure 2.1 shows the American S&P 500 index over the one year period from May 11th, 2010.

Options are a popular derivative on a specific asset, and are contracts between two parties, the buyer and the seller. The buyer, or holder, of the option has the right, but not the obligation to perform a future transaction on the underlying asset at a fixed price. For example, call options allow the holder to buy the underlying asset at a strike price K at maturity, or expiration, time T. This results in an effective payoff of

$$\text{call} = \max(S_T - K, 0), \tag{2.1}$$

where S_T is the price of the underlying asset at time T. Similarly, put options allow the holder the right to sell the underlying asset at time T and have an

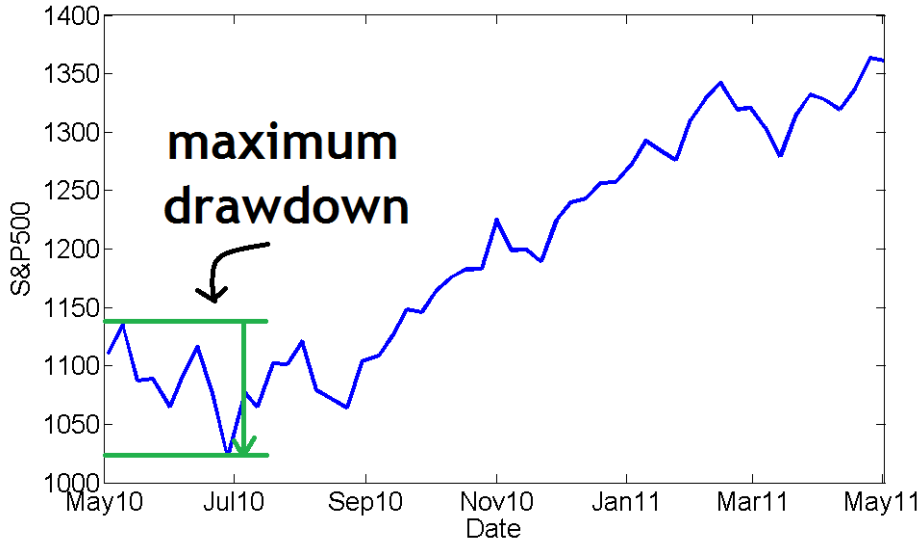

Figure 2.1: S&P 500 index realization over the one year period starting May 11, 2010.

effective payoff of

$$\text{put} = \max(K - S_T, 0). \tag{2.2}$$

Such options can only be exercised for the payoff at an exercises date. European options have only one exercise date at maturity, and can therefore only be exercised as the option expires. On the other hand, American options can be exercised at any time before maturity.

More complex options known as exotic options can be created with any desired payoff. Exotic options can be path-dependent and depend on the value of the asset at all times before maturity. A simple example is the lookback option, which depends on the extremum (maximum or minimum) of the asset value over its lifetime. In all cases, a fair price for such options must be determined and this gives rise to mathematical models.

2.1.1 Maximum Drawdown

In particular, this thesis focuses on a particular exotic option known as the maximum drawdown option. The maximum drawdown (*MD*) is the largest drop from a peak to a trough during the lifetime of the option. Figure 2.1 shows an example of this for the S&P 500 index. Mathematically, the maximum drawdown

at time t is given by,

$$MD(t) = \max_{0 \le u \le t} (M(u) - S(u)), \tag{2.3}$$

where $M(t)$ is the maximum,

$$M(t) = \max_{0 \le \alpha \le t} S(\alpha). \tag{2.4}$$

The European maximum drawdown option with strike K and maturity time T has payoff given by,

$$\text{payoff}_{MD} = \max(MD(\text{T}) - \text{K}, 0). \tag{2.5}$$

This can be viewed as an insurance product to the investor, since it protects his investment from maximum drawdowns larger than K.

2.1.2 Maximum Relative Drawdown

Closely related to the maximum drawdown is the maximum relative drawdown (*MRD*). Instead of an absolute drawdown, it is expressed as a ratio,

$$MRD(t) = \max_{0 \le u \le t} \left(1 - \frac{S(u)}{M(u)}\right). \tag{2.6}$$

This may be more intuitive to investors, who often deal in percentages of the underlying asset.

2.2 Stochastic Processes

In order to arrive at a fair price for the options described in Section 2.1, we first need to choose an appropriate model for the underlying asset. Since the future performance of the asset is unknown, it is natural to use a stochastic, or random process. This chapter will present and discuss some of the key models used in the financial industry.

2.2.1 Geometric Brownian Motion

Geometric Brownian motion (GBM) is the simplest and most widely used process in industry. The asset's path is described by the stochastic differential equation (SDE),

$$\frac{dS_t}{S_t} = \mu dt + \sigma dW, \tag{2.7}$$

where μ is the expected drift of the option, σ is the volatility, and W is a Brownian motion process. Intuitively, the first term is a constant growth term, while the

second is the source of randomness and risk. Although this model can be very successful in modelling many assets in the market, the simplest model assumes both constant μ and σ which often fluctuate in practice. The model also fails to account for the discontinuous jumps observed in the market. Note that GBM is only one choice and an entirely different model could be adapted.

2.2.2 Volatility Surface

One correction to the constant parameter problem is to allow for the volatility to vary as a function of the asset price and time. This is known as a volatility surface or a local volatility model. For our purposes we will generally work with constant volatility, but any volatility surface can be easily incorporated. This amounts to replacing σ in Equation (2.7) with the given surface $\sigma(S,t)$.

2.2.3 Stochastic Volatility

Although the volatility surface is an appropriate extension, it fails to account for the random behaviour of σ over time. As such it may be appropriate to use a second SDE for the volatility, known as stochastic volatility. Although we will not consider this model in the thesis, it is an appropriate extension to this work. As such it amounts to the modified SDEs,

$$\frac{dS_t}{S_t} = \mu dt + \sqrt{v_t} dW, \tag{2.8}$$

and

$$dv_t = \alpha(S,t)dt + \beta(S,t)dY, \tag{2.9}$$

where Y is a correlated Brownian motion process with correlation given by $dWdY = \rho dt$, and $\alpha(S,t)$ and $\beta(S,t)$ depend on the choice of model.

2.2.4 Jump-Diffusion

As discussed the GBM model fails to account for instantaneous jumps in the market, and we will show that this can produce significantly different results from a continuous model. As such we use the modified SDE,

$$\frac{dS_t}{S_t} = \mu dt + \sigma dW + (\eta - 1)dq_\lambda, \tag{2.10}$$

where dq_λ is an independent Poisson process with mean arrival time λ ($dq_\lambda = 0$ with probability $1 - \lambda dt$ and $dq_\lambda = 1$ with probability λdt), and η is the jump

amplitude causing S to jump to $S\eta$. The jump amplitude η has probability distribution function (PDF) $g(\eta)$.

In practice one can use any PDF for the jump distribution $g(\eta)$, but this thesis will focus on the log-normal distribution,

$$g(\eta) = \frac{e^{\left(-\frac{(\ln(\eta)-\mu_J)^2}{2\gamma^2}\right)}}{\sqrt{2\pi}\gamma\eta}, \tag{2.11}$$

with mean μ_J, and standard deviation γ.

Chapter 3

Risk-Neutral Valuation

Although the models of Chapter 2 are appropriate for modeling the underlying asset, our goal is to determine a fair price for options and financial derivatives. This is done by the concept of no-arbitrage, which states that there should not be a price difference between two equivalent products or strategies, because this could lead to an instantaneous risk-free profit. Black and Scholes showed that an option can be replicated by holding shares in the underlying asset and continuously rebalancing the amount of shares [22].

3.1 Partial Differential Equations

3.1.1 Black Scholes Equation

No-arbitrage applied to the GBM model results in a partial differential equation (PDE) known as the Black-Scholes equation. Given an option on an underlying no-arbitrage states that its price, V, is given by,

$$V_\tau = \frac{1}{2}\sigma^2 S^2 V_{SS} + rSV_S - rV, \tag{3.1}$$

where r is the risk free interest rate and $\tau = T - t$, where T is the expiry time. Note that r is the same for any underlying, and μ does not appear. For the purposes of this thesis we will consider only the case of constant r, but one could adopt a stochastic model for the interest rate. Such models are usually referred to as short rate models. This equation holds for any option on an underlying asset, and the specific option payoff will determine the boundary and terminal condition to be discussed in a later chapter. Although this equation has analytic solutions for simple (vanilla) options, for the case of the maximum drawdown option that is our focus, numerical techniques must be used.

3.1.2 Jump-Diffusion Equation

Under the jump-diffusion model an extension of the Black-Scholes equation arises, where the option value, V, is given by the partial integro differential equation (PIDE),

$$V_\tau = \frac{1}{2}\sigma^2 S^2 V_{SS} + (r - \lambda\kappa)SV_S - (r+\lambda)V + \lambda\int_0^\infty V(S\eta)g(\eta)d\eta, \tag{3.2}$$

where $\kappa = \mathrm{E}[\eta - 1]$, and $g(n)$ is the log-normal jump size density given in Equation (2.11). For compactness we will usually write Equation (3.2) as

$$V_\tau = \mathcal{L}V + \lambda\mathcal{J}V, \tag{3.3}$$

where

$$\mathcal{L}V = \frac{1}{2}\sigma^2 S^2 V_{SS} + (r - \lambda\kappa)SV_S - (r+\lambda)V, \tag{3.4}$$

and

$$\mathcal{J}V = \int_0^\infty V(S\eta)g(\eta)d\eta. \tag{3.5}$$

3.2 Risk Neutral Measure

An equivalent way of arriving at the Black-Scholes equation is to change the probability measure. While the equations of Chapter 2 are under the real-world ($\mathbb{P}$) measure, where the parameters are inferred from historical data, we can adopt a risk-neutral measure under which all assets drift at the risk neutral rate. Typically referred to as the $\mathbb{Q}$ measure, the parameters are instead found by calibrating to quoted option prices in financial markets.

3.3 Monte Carlo Methods

Under the risk neutral measure, an alternative to solving the associated PDE (or PIDE) is by Monte Carlo (MC) simulation. The value of the option is given by,

$$V = e^{-rT}\mathrm{E}^{\mathbb{Q}}[\text{payoff}], \tag{3.6}$$

where $\mathrm{E}^{\mathbb{Q}}[\text{payoff}]$ is the expected payoff under the risk neutral measure. By simulating M sample paths or realizations, we can approximate the expected value of a given future payoff as,

$$E^{\mathbb{Q}}[\text{payoff}] = \lim_{M\to\infty}\frac{\sum_{i=0}^{M}\text{payoff}_i}{M}, \tag{3.7}$$

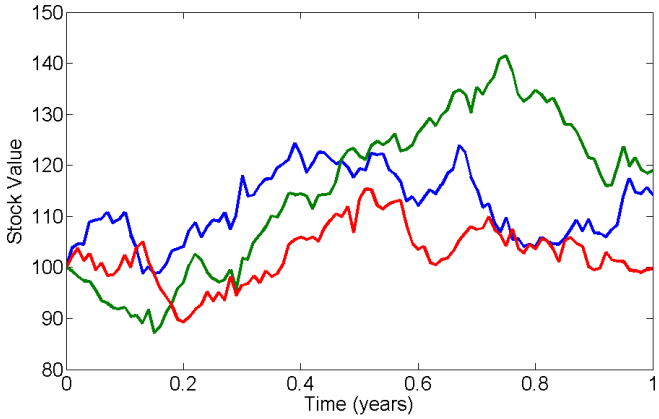

Figure 3.1: Monte Carlo simulated paths under GBM.

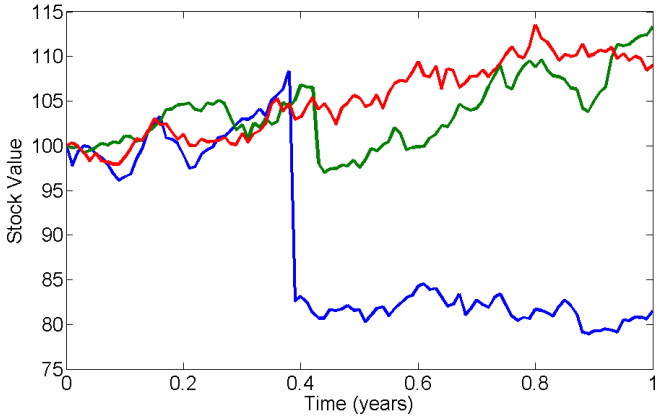

Figure 3.2: Monte Carlo simulated paths under jump-diffusion.

where payoff$_i$ is the simulated payoff of path i. We will focus primarily on numerical methods for solving the PIDE in Equation (3.2), but will use this technique for independent validation of our results where previous work has not been done. Figure 3.1 shows three such paths under GBM, and Figure 3.2 shows three paths under jump-diffusion. In practice of course three is not sufficient and millions of simulations often become necessary to achieve desired accuracy.

Chapter 4

Observation Conditions

4.1 Path-Dependent Options

Path-dependent options have payoffs depending in some way on the path of the option. For example, the option may depend on the average of the stock price or on the extrema during the lifetime of the option. In the stock market, the asset price can change every second, and investors can impact the price by buying or selling a significant number of shares. As a result, updating the average or extrema every instant is not necessarily the most appropriate action, since investors could take advantage of this quite easily.

We model the option with discrete observation times where the running payoff is updated a fixed number of times per year (N_{obs}). Our results will show that the continuously observed option can have a significantly different price than the discretely observed case even in the limit of daily observations. In general we work with a set of observation times $D = \left\{d_1, d_2, ..., d_{N_{\text{obs}}}\right\}$ at which point the path-dependent variables of the option are updated. Usually in practice $d_1 = 0$ and $d_{N_{\text{obs}}} = T$ since this is when the option is bought and exercised, respectively. For simplicity we will maintain a fixed observation interval,

$$\Delta d = \frac{T}{N_{\text{obs}}} \tag{4.1}$$

in all results throughout this thesis.

4.2 Partial Differential Equation

Given a PDE for the option value, we wish to solve for the value of a discretely observed path-dependent option. Unfortunately, since the PDE is solved backwards in time we do not know the path of the option. To work around this, we

introduce state variables from which we can calculate the option payoff. For arbitrary payoff, we write

$$V = V(S, t, Z), \tag{4.2}$$

where Z is a set of state variables which allow us to determine the payoff of the option. Hence for a payoff on the maximum we might require one state variable for the running maximum. The solution of the PDE then requires a set of observation conditions to update Z appropriately at each observation time d_i.

4.3 Observation Conditions

Given an observation time d_i, we denote the instant before and after the observation condition as d_i^- and d_i^+, respectively. The observation condition is,

$$Z^+ = f(Z^-, S, d_i), \tag{4.3}$$

where $Z^- = Z(d_i^-)$ is the set of state variables before the update, and $Z^+ = Z(d_i^+)$ is the state vector immediately after. The function f depends on the option type and explicit examples for the maximum drawdown will follow.

Across these observation times, we also need to update the option value. To do this we again apply a no-arbitrage condition, namely that

$$V(S, t^-, Z^-) = V(S, t^+, Z^+), \tag{4.4}$$

since otherwise an investor could profit from the instantaneous difference in the option value. The overall solution is obtained by solving the PDE from each d_i to d_{i-1}, and applying the observation condition at each d_i in Equation (4.4).

4.4 Maximum-Drawdown

An option on the maximum drawdown with strike K has payoff given by Equation (2.5). In this case the additional state variables are M and MD (see Eqns (2.3) and (2.4)) and $Z = \{M, MD\}$ and $V = V(S, t, M, MD)$.

The full problem is solved on the three-dimensional domain, $0 < S < M < \infty$, $0 \leq MD < \infty$ and $0 \leq t \leq T$, where $V = V(S, t, M, MD)$ and M and MD are updated only at a set of observation times D. In the case of the maximum drawdown, given the asset price S, these observation conditions are

$$M^+ = \max(M^-, S), \tag{4.5}$$

and

$$MD^+ = \max(MD^-, M^+ - S), \tag{4.6}$$

where $M^\pm = M(d_i^\pm)$, and $MD^\pm = MD(d_i^\pm)$. Since we solve the PDE backwards through time, we initially set $M^-(d_{N_{\text{obs}}}) = M(t = T)$ and $MD^-(d_{N_{\text{obs}}}) = MD(t = T)$. From no arbitrage, we have that the option value must not change from this condition, and hence,

$$V(S, t = d_i^-, M^-, MD^-) = V(S, t = d_i^+, M^+, MD^+). \tag{4.7}$$

Substituting Equation (4.5) and (4.6) into Equation (4.7), we obtain

$$V(S, t = d_i^-, M^-, MD^-) = V(S, t = d_i^+, \max(M^-, S), \max\left(MD^-, \max(M^-, S) - S\right). \tag{4.8}$$

4.5 Maximum-Relative Drawdown

The situation is very similar for the maximum relative drawdown [17], which is given by Equation (2.6). The payoff, in this case is

$$\text{payoff}_{MRD}(MRD, K) = \max(MRD - K, 0). \tag{4.9}$$

Where the full problem is solved on the three-dimensional domain $0 < S < M < \infty$, $0 \leq MRD < 1$ and $0 \leq t \leq T$, where $V = V(S, t, M, MRD)$ and M and MRD are updated only at a set of observation times, D. The new observation conditions become,

$$MRD^+ = \max(MRD^-, 1 - S/M^+), \tag{4.10}$$

and

$$V(S, t = d_i^-, M^-, MRD^-) = V(S, t = d_i^+, \max(M^-, S), \max\left(MRD^-, 1 - S/\max(M^-, S)\right). \tag{4.11}$$

The maximum relative drawdown may be more intuitive to investors, since it is naturally expressed as a fraction of the underlying asset. Furthermore, we will also show that, numerically, it has some advantages since, even in the case of arbitrary strike, we can reduce the dimensionality of the problem by a similarity reduction. As described in Section 4.3, we solve a set of 1-D PDEs coupled with the observation condition in Equation (4.11) at fixed observation times D.

Chapter 5

Boundary and Payoff Conditions

In order to solve the PIDE in Equation (3.2), we need an appropriate payoff (terminal) condition, and boundary conditions at $S = 0$ and $S = \infty$. The payoff is given by the option type, and in general may depend on S and the set of additional state variables Z. Since there is no direct dependence in the PIDE on the state variables in Z, we require no additional boundary conditions. The dependence on these state variables comes solely through the observation conditions discussed in Chapter 4.

5.1 Boundary Conditions

As $S \to 0$, Equation (3.2) becomes

$$V_\tau = -rV, \tag{5.1}$$

because $g(\eta)$ is a probability density function and we assume that V is bounded near $S = 0$, which gives $S^2 V_{SS} \to 0$ as $S \to 0$. Indeed, if we assume a non-zero value of $S^2 V_{SS}$ at $S = 0$, then

$$V_{SS}(S = 0) = O\left(\frac{1}{S^2}\right). \tag{5.2}$$

Integrating would give,

$$V(S = 0) = O(\log S) + aS + b, \tag{5.3}$$

but then V could not be bounded.

As $S \to \infty$, we could apply the linearity condition $V_{SS} = 0$ [23]. However, as discussed in [18], this no longer leads to a monotone scheme. Applying this directly to Equation (3.2) we obtain,

$$V_\tau = rSV_S - rV, \tag{5.4}$$

which we can apply for any option type.

Alternatively, integrating $V_{SS} = 0$ twice gives,

$$V = c(t, Z)S + b(t, Z). \tag{5.5}$$

Using Equation (5.5) in Equation (3.2), we obtain $c_\tau = 0$ and $b_\tau = -rb$. However, the precise functions c and b are given by the specific option type. We will show examples of this technique for the maximum drawdown and maximum relative drawdown.

5.2 Maximum Drawdown

In order to solve Equation (3.3), we need appropriate boundary and payoff conditions. The payoff condition for the maximum drawdown is,

$$V(S, T, M, MD, K) = \text{payoff}_{MD}(MD, K). \tag{5.6}$$

For large S we expect the option value to be linearly proportional to S from the definition of the maximum drawdown in Equation (2.3). As a result, we make the assumption that in Equation (5.5), $b \ll cS$, which gives

$$V = c(t, M, MD)S \tag{5.7}$$

as $S \to \infty$, and

$$V_\tau = 0. \tag{5.8}$$

This is equivalent to applying a Dirichlet condition, and preserves the monotonicity of our scheme. In practice using either Equation (5.4) or (5.8) for the boundary condition gives the same result to accuracy well below the discretization error.

5.3 Maximum Relative Drawdown

For the case of the relative maximum drawdown, *MRD*, the boundary conditions are similar with terminal condition payoff_{MRD} instead of payoff_{MD}. As $S \to \infty$ we can apply $V_{SS} = 0$ directly, or by integrating we have

$$V = c(t, M, MRD)S + b(t, M, MRD). \tag{5.9}$$

Since the drawdown is relative, we expect V to be independent of S for large S. As a result, we assume $c = 0$, and we have

$$V_\tau = b_\tau = -rV, \tag{5.10}$$

as at $S = 0$. This is equivalent to applying a time-dependent Dirichlet condition, and preserves the monotonicity of the scheme. As with the maximum drawdown, both methods give the same result to accuracy well below the discretization error.

Chapter 6

Similarity Reduction

With an abuse of notation, we will write $V = V(S, t, Z_1, Z_2)$ when considering observation conditions, but $V = V(S, \tau, Z_1, Z_2)$ in the context of the PIDE solve. Since the discrete path-dependent problem requires the use of additional state variables, the problem becomes multi-dimensional. In order to reduce the overall complexity of the problem, we employ what is called a similarity reduction. A PIDE satisfies a general similarity reduction of degree n if the solution V satisfies,

$$V(\zeta S, \tau, \zeta Z_1, Z_2) = \zeta^n V(S, \tau, Z_1, Z_2), \tag{6.1}$$

where Z_1 is a set of variables affected by the similarity reduction, Z_2 is a set of variables unaffected and $\zeta > 0$ is an arbitrary constant. Each valid similarity reduction allows one variable from Z_1 to be removed, reducing the overall dimensionality. Alternatively, a similarity reduction of degree n is valid if, given a solution $V(S, \tau, Z_1, Z_2)$, $\frac{1}{\zeta^n}\hat{V}(\zeta S, \tau, \zeta Z_1, Z_2)$ is also a solution. This follows because the solution is unique and we then have that $\hat{V}(\zeta S, \tau, \zeta Z_1, Z_2) = V(\zeta S, \tau, \zeta Z_1, Z_2)$.

6.1 PIDE

We begin with a more general form of the PIDE in Equation (3.2),

$$V_\tau = c_1 S^2 V_{SS} + c_2 S V_S + c_3 V + c_4 \int_0^\infty V(S\eta, t, Z_1, Z_2) g(\eta), \tag{6.2}$$

where c_1,c_2,c_3, and c_4 are independent of S. Assuming Equation (6.1) holds, we then have by a change of variables $V(S, \tau, Z_1, Z_2) = \frac{1}{\zeta^n}\hat{V}(\hat{S}, \tau, \hat{Z}_1, Z_2)$ is also a solution, where $\hat{S} = \zeta S$, and $\hat{Z}_1 = \{\zeta z \mid \forall z \in Z_1\}$. This follows from straightforward

substitution into Equation (6.2),

$$\begin{aligned}\frac{1}{\zeta^n}\hat{V}_\tau &= c_1 S^2\zeta^2\frac{1}{\zeta^n}\hat{V}_{\hat{S}\hat{S}} + c_2 S\zeta\frac{1}{\zeta^n}\hat{V}S + c_3\frac{1}{\zeta^n}\hat{V} + c_4\frac{1}{\zeta^n}\int_0^\infty \hat{V}(\hat{S}\eta,\tau,\hat{Z}_1,Z_2)g(\eta)d\eta \\ \hat{V}_\tau &= c_1\hat{S}^2\hat{V}_{\hat{S}\hat{S}} + c_2\hat{S}\hat{V}_{\hat{S}} + c_3\hat{V} + c_4\int_0^\infty \hat{V}(\hat{S}\eta,\tau,\hat{Z}_1,Z_2)g(\eta)d\eta.\end{aligned}$$

In addition to this, we require that the associated boundary and terminal conditions also admit a similarity solution. Since these depend on the specific option problem, we will provide the examples for the maximum drawdown and maximum relative drawdown.

6.2 Observation Conditions

When pricing discretely observed options, the similarity reduction must also be maintained under observation conditions. Namely, we assume the reduction holds before the update at t^+,

$$V(S,t^+,Z_1^+,Z_2^+) = \frac{1}{\zeta^n}V(\zeta S,t^+,\zeta Z_1^+,Z_2^+), \tag{6.3}$$

and need to prove that it holds after the update. As a result we must show that

$$V(S,t^-,Z_1^-,Z_2^-) = \frac{1}{\zeta^n}V(\zeta S,t^+,\zeta Z_1^+,Z_2^+). \tag{6.4}$$

Once again, since the observation conditions depends on the specific problem, we will provide examples for the maximum drawdown and maximum relative drawdown.

6.3 Maximum Drawdown

Although the solution to Equation (3.2) for the maximum drawdown requires the use of three state variables (S,M,MD), and is hence a three-dimensional problem, it can often be reduced to a two-dimensional problem through a similarity reduction of degree one. Using the notation of this chapter, we define $Z_1 = \{M,MD\}$, $Z_2 = \emptyset$ and $n = 1$.

To show that the problem admits a similarity reduction, we first show that the reduction holds at maturity. Namely, for the cases of no strike, $K = 0$, we have at maturity, from Equation (5.6),

$$V(S,T,M,MD) = MD = \frac{1}{\zeta}V(\zeta S,T,\zeta M,\zeta MD). \tag{6.5}$$

Furthermore, the PIDE given in Equation (3.2) admits a similarity solution, as mentioned in Section 6.1.

Finally, we show that the similarity reduction is maintained under the observation update rule in Equations (4.7). Given a similarity solution, the observation condition is,

$$V(\zeta S, t^-, \zeta M^-, \zeta MD^-) = V(\zeta S, t^+, M^+(\zeta S, \zeta M^-, \zeta MD^-), MD^+(\zeta S, \zeta M^-, \zeta MD^-)), \tag{6.6}$$

where from conditions (4.5 and 4.6) we have,

$$M^+(\zeta S, \zeta M^-, \zeta MD^-) = \zeta M^+(S, M^-, MD^-), \tag{6.7}$$

and

$$MD^+(\zeta S, \zeta M^-, \zeta MD^-) = \zeta MD(S, M^-, MD^-). \tag{6.8}$$

Hence, Equation (6.6) becomes,

$$\begin{aligned} V(\zeta S, t^-, \zeta M^-, \zeta M^+) &= V(\zeta S, t^+, \zeta M^+, \zeta MD^+) \\ &= \zeta V(S, t^+, M^+, MD^+) \\ &= \zeta V(S, t^-, M^-, MD^-), \end{aligned} \tag{6.9}$$

by Equation (6.3) and the observation condition of Equation (4.7). As a result, we have that the similarity reduction is preserved under the observation conditions.

Since the similarity reduction holds for the payoff at time $t = T$, and is preserved under the PIDE and observation conditions, we have that the reduction holds for all time $0 \leq t \leq T$,

$$V(S, t, M, MD) = \frac{1}{\zeta} V(\zeta S, t, \zeta M, \zeta MD). \tag{6.10}$$

By choosing $\zeta = M^*/M$, we have that,

$$V(S, t, M, MD) = \frac{M}{M^*} V(S\frac{M}{M^*}, t, M^*, \frac{M^*}{M} MD). \tag{6.11}$$

As a result, we can solve for one particular value of M, namely M^*, and find the solution for all values of M solving a two-dimensional problem. Note that for an arbitrary strike, the option value does not have this scaling property, and the full three-dimensional problem must be solved.

6.4 Maximum Relative Drawdown

For the maximum relative drawdown we define $Z_1 = \{M\}$ and $Z_2 = \{MRD, K\}$, this allows a similar argument to be made for the MRD using Equations (3.2),

(4.9) and (4.11) which gives that for arbitrary strike K,

$$V(S,t,M,MRD,K) = V(\zeta S,t,\zeta M,MRD,K). \tag{6.12}$$

Using the same value for ζ, we obtain

$$V(S,t,M,MRD,K) = V(S\frac{M}{M^*},t,M^*,MRD,K). \tag{6.13}$$

As a result, even in the case of arbitrary strike, the *MRD* case can still be reduced to two-dimensions. Note that the strike K is a parameter induced by the payoff, and does not add to the dimensionality of the problem.

Chapter 7

Numerical Solution

The focus of this thesis is on the numerical solution of the maximum drawdown and maximum relative drawdown options, and the finite difference method used for the solution is described in this Chapter. We will discuss the localization, discretization, convergence and also the choice of grid type and interpolation method for the observation conditions.

7.1 Localization

In order to solve the problem numerically, we first localize to a finite domain. For the maximum drawdown, we solve the problem on $0 \leq S \leq S_{\max}$, $0 \leq M \leq M_{\max}$, and $0 \leq MD \leq MD_{\max}$. For the maximum relative drawdown, we solve the problem on the localized domain, with $0 \leq S \leq S_{\max}$, $0 < M_{\min} \leq M \leq M_{\max}$, and $0 \leq MRD \leq 1$. Forcing $M_{\min} > 0$ ensures that the MRD is defined and bounded on our localized domain. Given that we localize the problem to a finite domain, it is necessary to discuss adjustments to the observation conditions and boundary conditions presented in Sections 4.4 and 5. In addition, we need be sure to select $S_{\max}$, $M_{\max}$, and $MD_{\max}$ sufficiently large to avoid introducing significant localization error in the interior. Similarly, for the maximum relative drawdown, we select sufficiently large $MRD_{\max}$ and sufficiently small $M_{\min}$.

7.1.1 Observation Condition Localization

For both the maximum drawdown and maximum relative drawdown, if $S_{\max} > M_{\max}$, then it is possible that $M^+ > M_{\max}$, in which case the observation condition on M given in Equation (4.5) uses information outside the localized domain. Instead of extrapolating, we simply obtain information from the largest available

node,

$$M^+ = \min\left(\max(M^-, S), M_{\max}\right). \tag{7.1}$$

The effect of this is similar to localizing the domain and has an insignificant impact on solution values for $M_{\max}$ large. This is verified computationally by increasing the value of $M_{\max}$ and showing an insignificant change, relative to the discretization error, to the solution in the interior.

In addition, for the maximum drawdown it is possible that $MD^+ > MD_{\max}$, so we make the modification

$$MD^+ = \min\left(\max(MD^-, M^+ - S), MD_{\max}\right). \tag{7.2}$$

Similarly as for the maximum relative drawdown, it is possible that $MRD^+ > MRD_{\max}$, so we modify the observation condition to

$$MRD^+ = \min\left(\max(MD^-, M^+ - S), MRD_{\max}\right). \tag{7.3}$$

Again in these instances we verify computationally that $MD_{\max}$ and $MRD_{\max}$ are sufficiently large so that the error introduced to the interior is insignificant relative to the discretization error.

7.1.2 Boundary Condition Localization

We also need to localize the boundary condition as $S \to \infty$ to $S = S_{\max}$. Here we make the same assumption that $S_{\max}$ is sufficiently large so that our assumptions in Section 5 hold. Namely we expect one of Equations (5.4), (5.8) or (5.10) to hold at $S = S_{\max}$.

7.2 Discretization

A finite difference method results in a specific discretized form of the PIDE in Equation (3.3). Given a discretization of the localized interval of each variable, we can then discretize the PIDE. Between the observation dates, we can use either Crank-Nicolson (CN) or fully-implicit timestepping to solve the 1-D PDE. For the full-jump diffusion model we follow the method presented by d'Halliun *et al.* [24] which uses a fixed point iteration and FFT evaluation of the jump integral.

Specifically, the discretized form of Equation (3.3) is,

$$\frac{V^{n+1} - V^n}{\Delta\tau} = \mathcal{L}^h\left(\theta V^{n+1} + (1-\theta)V^n\right) + \lambda\mathcal{J}^h\left(\theta V^{n+1} + (1-\theta)V^n\right), \tag{7.4}$$

where $\theta = 1$ for implicit timestepping, $\theta = 1/2$ for CN timestepping, and V^n is the column-vector

$$V^n = \begin{bmatrix} V_1^n & \dots & V_i^n & \dots & V_{N_S}^n \end{bmatrix}^T, \tag{7.5}$$

where $V_i^n = V(S_i, t_n, M, MD)$. In matrix form, we write $\mathcal{L}^h V^n$ as

$$\mathcal{L}^h V^n = -AV^n, \tag{7.6}$$

where A is an $\mathcal{M}$-matrix with entries

$$A_{ij} = \begin{cases} -\alpha_i & j = i-1 \\ r + \lambda + \alpha_i + \beta_i & j = i \\ -\beta_i & j = i+1 \\ 0 & otherwise \end{cases}, \tag{7.7}$$

Here α_i and β_i are given in [25] and depend on the type of finite-difference approximations used. Note that we use central differencing as much as possible, but apply forward or backward differencing to ensure $\alpha_i, \beta_i \geq 0$. The discrete jump term, $\mathcal{J}^h V^n$ is given precisely in [24] but is an approximate FFT evaluation of the integral,

$$I(S) = \int_0^\infty V(S\eta, t_n, M, MD) g(\eta) d\eta. \tag{7.8}$$

To avoid solving a dense matrix, we use the fixed point iteration scheme in [24]. Let $\hat{V}^k$ be the k^{th} iterate for V^{n+1}. We solve for V^{n+1} using the iteration,

$$[I + \theta\Delta\tau A]\,\hat{V}^{k+1} = [I - (1-\theta)\Delta\tau A]\,V^n + \theta\Delta\tau\lambda\mathcal{J}^h\hat{V}^k + (1-\theta)\Delta\tau\lambda\mathcal{J}^h V^n, \tag{7.9}$$

where we use an FFT method [24] to evaluate the dense matrix vector multiply $\mathcal{J}^h\hat{V}^k$.

7.2.1 Maximum Drawdown

For the particular case of the maximum drawdown, the state variables M and MD are discretized on the intervals $[0, M_{\max}]$ and $[0, MD_{\max}]$, respectively, where $M_{\max}$ and $MD_{\max}$ are chosen to be sufficiently large to avoid significant localization error. We denote the number of nodes in the S, M, and MD directions by N_S, N_M and N_{MD} respectively. By solving Equation (3.3) for each grid node, (M_j, MD_k) we advance the solution to each observation date, where we apply the observation conditions given in Section 4.4.

7.2.2 Maximum Relative Drawdown

The methodology is similar for the maximum relative drawdown as for the maximum drawdown in Section 7.2.1, but here we take special care to ensure that the discretization for M does not include zero as described in Section 7.1. As a result, we discretize M on the interval $[M_{\min}, M_{\max}]$ and MRD on the interval $[0,1]$, where $M_{\max}$ is chosen sufficiently large and $M_{\min}$ sufficiently small to avoid localization error. As for the maximum drawdown case, we denote the number of nodes in each direction as N_S, N_M, and N_{MRD}. The discretized PIDE and boundary conditions are the same as in Section 7.2.1, and we use the localized observation conditions for the maximum relative drawdown given in Section 7.1.1 and Equation 4.11.

7.3 Convergence

In order to guarantee convergence for our discretization, we refer to [26], which states that *stability*, *monotonicity,* and *consistency* are sufficient conditions. Furthermore, [27] establishes *monotonicity* and *consistency* for a general jump-diffusion PIDE of the form in Equation (3.2). Following this it is clear that our scheme also satisfies *monotonicity* and *consistency* and we simply need to show that our scheme is also *stable*.

7.4 Stability

Between observation times, the discretization used is unconditionally stable for the case of fully implicit timestepping between observation dates as discussed in [24], since we use a positive coefficient method. Similarly, the Crank-Nicolson timestepping is algebraically stable as shown in [24]. In order to guarantee stability for the entire scheme, we must also show that the observation conditions and similarity reduction preserve stability.

7.4.1 Observation Conditions

The observation conditions preserve stability if we can bound the observation conditions as described in Section 7.1.1. For the full three dimensional problem, it is easily shown that

$$V(S, d_i^-, M^-, MD^-) \leq ||V(S, d_i^+)||_\infty, \tag{7.10}$$

where $||V(S, d_i^+)||_\infty = \max_{M,MD} V(S, d_i^+, M, MD)$ over all (M, MD) grid pairs.

7.4.2 Observation Conditions with Similarity Reduction

Using the similarity reduction however, the impact of the observation conditions require further analysis. In particular, if $M^+ > M^*$, then $\zeta < 1$, from Equation (6.9) and Equation (7.10) may not hold.

Instead, we modify the update condition of Equation (4.7) slightly to become,

$$V(S, t^-, M^-, MD^-) = \min(V(S, t^+, M^+, MD^+), MD_{\max}). \tag{7.11}$$

In this case we trivially have $V(S, t^-, M, MD) \leq MD_{\max}$ and stability is therefore guaranteed.

The cap on V is chosen to be $MD_{\max}$, because without similarity reduction this is the largest value the numerical solution can have when restricted to the finite domain $[0, S_{\max}] \times [0, M_{\max}] \times [0, MD_{\max}]$. The effect of this is similar to the localization conditions described in Section 7.1 and in Section 8.3 we will show that this has an insignificant impact on solution values away from the boundary. This is further verified by increasing the value of $MD_{\max}$ and showing an insignificant change to the solution.

7.4.3 Maximum Relative Drawdown

For the full three dimensional problem, the maximum relative drawdown is also unconditionally stable under observation conditions, where we have

$$V(S, d_i^-, M^-, MRD^-) \leq ||V_{MRD}(S, d_i^+)||_\infty, \tag{7.12}$$

with $||V_{MRD}(S, d_i^+)||_\infty = \max_{M,MRD} V(S, d_i^+, M, MRD)$ over all (M,MRD) grid pairs. It is also trivially stable under observation conditions with the similarity reduction since the reduction is homogeneous of degree zero as given by Equation (6.13).

7.5 Grid

Before choosing a grid, it is important to identify the characteristics of the look-up operation at each observation date. From Equations (4.5) and (4.6), as illustrated in Figures 7.1 and 7.2, all look-up operations draw from a single line. When $M^+ = M^-$ or $MD^+ = MD^-$ we say that the look-up in the given direction is stationary. Since one of Equations (4.5) and (4.6) will always be stationary, at most one of M or MD will change. Although we can avoid any interpolation by using a uniform grid as depicted in Figure 7.2, a non-uniform grid can allow for faster convergence to the particular region of the desired solution.

Furthermore, to achieve no interpolation, we would need identical nodes for S, M, and MD, which is only practical for M and S, since MD values are

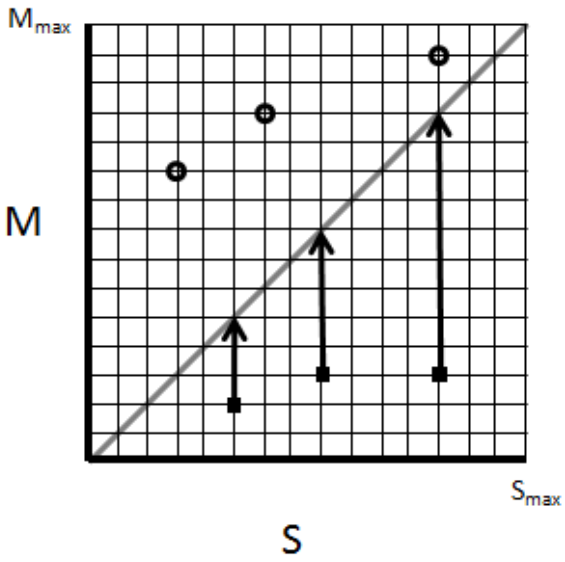

Figure 7.1: Information flow diagram for M. The square points represent values that once updated, take on the value of the diagonal line (grey). The arrows show the direction of the look-up, and the circular points are stationary, which remain unchanged across the observation date.

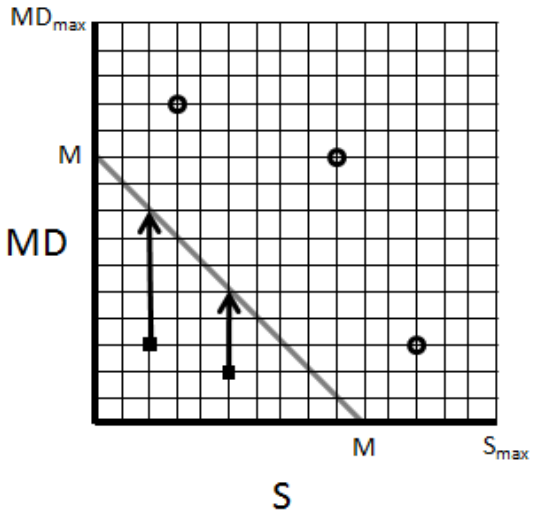

Figure 7.2: Information flow diagram for MD. The square points represent values that once updated, take on the value of the diagonal line (grey). The arrows show the direction of the look-up, and the circular points are stationary, which remain unchanged across the observation date.

significantly different in magnitude. Since options are initially sold at asset price $S = S_0$, it is desirable to scale the S-nodes near this value. As a result, we use a non-uniform grid in the S-direction, which is dense near S_0 and sparse near zero and $S_{\max}$. For a first approach, we use an M grid identical to S, namely, given

$$S^g = \{S_1^g, ..., S_i^g, ...S_{N_S}^g\} = M^g = \{M_1^g, ..., M_j^g, ...M_{N_M}^g\}, \tag{7.13}$$

where $S_i^g = M_j^g$, and $N_S = N_M$ is the number of S or M grid nodes. Using a simple uniform grid in the MD direction and taking the Cartesian product with M_g and S_g, we achieve a simple full grid which we will refer to as the *repeated* grid. The $M - S$ plane of this grid is depicted in Figure 7.3, where the nodes are more dense near $S = S_0$. There will be no interpolation error from the update rule in Equation (4.5), since either the look-up is stationary in M, or $M^+ = S$, which is guaranteed to exist since we use the same nodes for S and M ($S_g = M_g$).

Due to the discrete nature of the problem, and the fact that update rules draw frequently from the values near the diagonal, it has been shown that better convergence can be obtained by further increasing the density near the diagonal [18]. As a result, we extend the *repeated* grid to be more dense near $S = M$. This focuses the nodes near the look-up diagonal shown in the $M - S$ plane of Figure 7.2, which should improve the rate of convergence. We use the standard set of S-nodes from the *repeated* grid at $M = S_0$, $MD = 0$, and scale this with M elsewhere, ensuring that the $M = S$ node exists, and that the S grid is highest in density at this point. Given the S_{grid} used in the *repeated* grid, which is focused around S_0, the grid at a given M is,

$$S^M = \left\{ S_1^g \frac{M}{S_0}, ..., S_i^g \frac{M}{S_0}, ..., S_{N_S}^g \frac{M}{S_0} \right\}. \tag{7.14}$$

Note that although this scaling may improve accuracy due to increased density of nodes near the diagonal, it may cause a trade-off of increased interpolation error, which we will attempt to remedy in Section 7.6. This grid will be referred to as the *scaled* grid. and is depicted in Figure 7.4.

7.6 Observation Condition Interpolation

At each observation date the observation conditions are used to update the grid values, and interpolation may be necessary. Depending on the grid used, interpolation may occur more or less frequently. Interpolation is necessary when

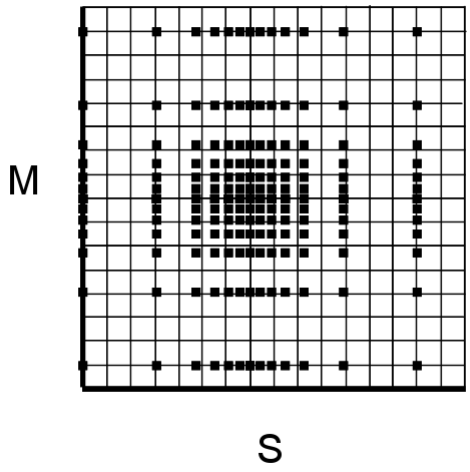

Figure 7.3: Depiction of the repeated grid in the M-S plane. The repeated grid is a Cartesian product where a fixed S_{grid} for both M and S is used.

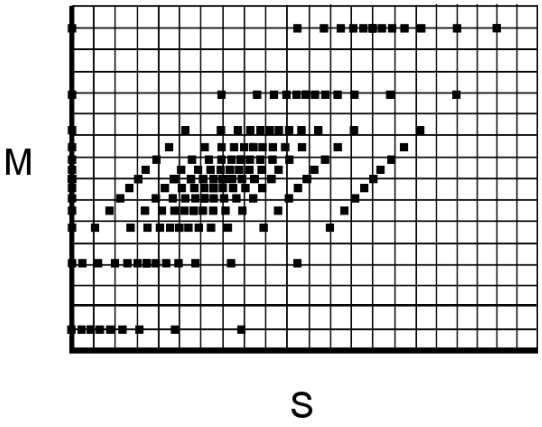

Figure 7.4: Depiction of the scaled grid in the M-S plane. The scaled grid has the modification that S_{grid} is scaled with S according to Equation (7.14).

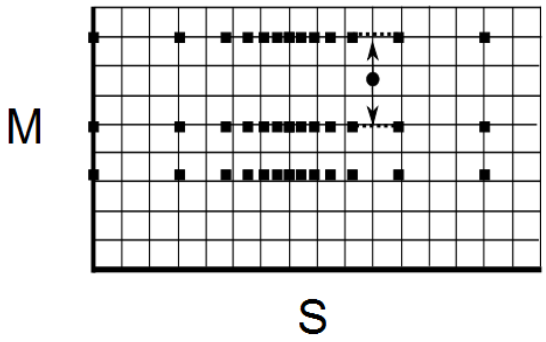

Figure 7.5: Depiction of linear interpolation method used for observation condition look-up.

(S, M^-, MD^-) is between grid nodes as depicted in Figure 7.2. In particular, when using the *repeated* grid described in Section 7.5, no interpolation in the M direction will be necessary. It is evident that standard trilinear interpolation can be used, as shown in Figure 7.5, interpolating along the S, M, and MD directions as necessary. Although this may be suitable for the *repeated* grid, we also consider diagonal interpolation, as shown in Figure 7.6 since it has been shown to be effective when using the *scaled* grids discussed previously [18]. For the M update rule, since nodes are dense near the diagonal where the interpolation occurs at $M = S$, we can interpolate along the direction of the line $M = S$ using

$$V(S, M = S) = V(S_{\text{lo}}, M = S_{\text{lo}}) + \frac{V(S_{\text{hi}}, S_{\text{hi}}) - V(S_{\text{lo}}, S_{\text{lo}})}{(S_{\text{hi}} - S_{\text{lo}})\sqrt{2}}(S - S_{\text{lo}})\sqrt{2}, \qquad (7.15)$$

where, given M, S_{lo} and S_{hi} are the closest nodes to S such that $S_{\text{lo}} \leq S \leq S_{\text{hi}}$. This is illustrated in Figure 7.6.

7.7 Alterations for Similarity Reduction Problem

In the case that the similarity reduction holds where we choose $\zeta = M^*/M$, we require a two-dimensional grid in only MD and S. As a result, we can use a similar *repeated* grid mentioned already, using S_g and a uniform MD grid, in a similar fashion to the full three-dimensional problem. Given that our only update

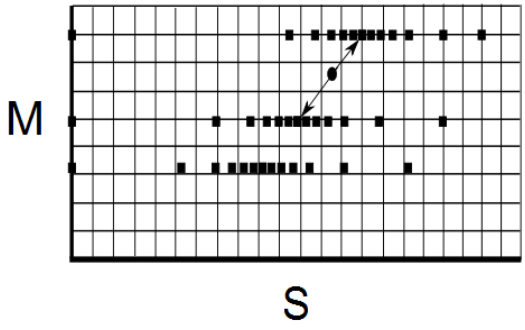

Figure 7.6: Depiction of diagonal interpolation method used for observation condition look-up.

interpolation is along $MD = M^* - S$, it is desirable to create a grid with nodes dense around this line, as in Section 7.5 for the $M = S$ line. To achieve this, we instead scale according to MD, (see Figure 7.2)

$$S^{MD} = \left\{ S_1^g \frac{M^* - MD}{S_0}, ..., S_i^g \frac{M^* - MD}{S_0}, ..., S_{N_S}^g \frac{M^* - MD}{S_0} \right\}, \tag{7.16}$$

and apply an analogous diagonal interpolation as described in Section 7.6 along the line $MD = M^* - S$,

$$V(S, MD = M^* - S) = V(S_{\text{lo}}, M^* - S_{\text{lo}}) + \frac{V(S_{\text{hi}}, M^* - S_{\text{hi}}) - V(S_{\text{lo}}, M^* - S_{\text{lo}})}{(S_{\text{hi}} - S_{\text{lo}})\sqrt{2}} (S - S_{\text{lo}})\sqrt{2}. \tag{7.17}$$

We will refer to this as the *MD-scaled* grid.

7.8 Alterations for Maximum Relative Drawdown

In the case of the maximum relative drawdown problem, a few minor adaptation are necessary. Both the *repeated* and *scaled* grids mentioned in Section 7.5 are directly analogous, and only the values of the MD need to be replaced with appropriate MRD values.

The similarity reduction is also slightly different for the maximum relative drawdown, as given in Equation (6.13). As a result, we can create a *MRD-scaled* grid by scaling appropriately,

$$S^{MRD} = \left\{ S_1^g \frac{M^*(1 - MRD)}{S_0}, ..., S_i^g \frac{M^*(1 - MRD)}{S_0}, ..., S_{N_S}^g \frac{M^*(1 - MRD)}{S_0} \right\}, \tag{7.18}$$

and by applying an analogous diagonal interpolation

$$V(S, MRD = 1-S/M^*) = V\left(S_{\text{lo}}, 1-\frac{S_{\text{lo}}}{M^*}\right)+\frac{V\left(S_{\text{hi}}, 1-\frac{S_{\text{hi}}}{M^*}\right)-V\left(S_{\text{lo}}, 1-\frac{S_{\text{lo}}}{M^*}\right)}{(S_{\text{hi}}-S_{\text{lo}})\sqrt{2}}(S-S_{\text{lo}})\sqrt{2}. \tag{7.19}$$

Chapter 8

Results

In this Chapter we give results for various problem parameters and study the effects of grid choice, similarity reduction and timestepping. All convergence studies are performed for a discretely observed option unless otherwise stated.

8.1 Effect of Grid / Interpolation Type

We investigate the effects of the *scaled* grids mentioned in Section 7.5, as well as the type of interpolation from update conditions. The results of this convergence testing are given in Table 8.2, using the data in Table 8.1 modelled without jumps. We start with a coarse grid of 35 S and M nodes, and 20 MD nodes. At each refinement, we double the number of timesteps and insert new nodes half way between each existing pair of nodes.

The results show that the *scaled* grids achieve better convergence when compared to the *repeated* grids, despite the additional interpolation error from the M update rule. On the other hand, unlike [18], we observe that diagonal interpolation does not improve the convergence. In fact, this is reasonable since in the case of the cliquet option in [18], under the similarity reduction the interpolation was exact, which is not the case for the maximum drawdown here. As a result, we will use *scaled* grids with linear interpolation unless otherwise specified.

8.2 Localization Error

Using the data in Table 8.1 once more, we investigate the effects of a finite $S_{\max}$, $M_{\max}$ and $MD_{\max}$. Specifically, we use the *scaled* grid from Section 8.1 with the largest node in each direction scaled by a factor of 10. If we denote the new grid

Parameter	Value
S_0	100
T	1.5
σ	0.2
r	0.04
N_{obs}	5
λ	0
$S_{\max}$	1800
$M_{\max}$	1800
$MD_{\max}$	1000

Table 8.1: Parameters used for Black-Scholes model without jumps.

N_S, N_M, N_{MD}	N	Scaled Grids (diagonal interp)	Scaled Grids (linear interp)	Repeated Grid
35,35,20	60	15.4197	15.9271	14.6272
70,70,40	120	15.9193	16.0744	15.6249
140,140,80	240	16.0785	16.1204	16.0049

Table 8.2: Comparison of grid type and interpolation methods for the discrete MD no-jump case using the parameters in Table 8.1. Full three dimensional grid.

N_S, N_M, N_{MD}	Timesteps	Value
35,35,20	60	15.9271
64,64,40	120	16.0744
128,128,80	240	16.1204

Table 8.3: Results using *scaled* grid with linear interpolation with increased $S_{\max}$, $M_{\max}$, and $MD_{\max}$ (see Equation (8.1)). The values for the *MD* with no-jumps are in agreement to at least six significant digits compared with Table 8.2.

maximums, $\hat{S}_{\max}$, $\hat{M}_{\max}$, and $\hat{MD}_{\max}$, then,

$$\begin{aligned} \hat{S}_{\max} &= 10S_{\max} \\ \hat{M}_{\max} &= 10M_{\max} \\ \hat{MD}_{\max} &= 10MD_{\max}. \end{aligned} \tag{8.1}$$

Note that in the *scaled* grid, the $S_{\max}$ also varies with M.

From the results for the enlarged grid shown in Table 8.3, we see that the solution is the same as in Table 8.2 to at least six significant digits. This indicates that the localization error is significantly smaller than the discretization error.

8.3 Effect of Similarity Reduction

In the case of constant volatility, the similarity reduction is valid for the maximum drawdown with $K = 0$, and for the maximum relative drawdown with arbitrary strike, K. In these cases we can reduce both the computational and spatial complexity. We investigate the convergence with the similarity reduction applied for the same data given in Table 8.1 (no jumps). Table 8.4 shows the results using the similarity reduction. Although under the similarity reduction we use the *MD-scaled* grids as opposed to the standard *scaled* grids, the results are similar to Table 8.2 and we therefore use the analagous *MD-scaled* grids with linear interpolation for the similarity reduction.

Comparing the results in Table 8.4 with Table 8.2, we can see that both methods, as expected, appear to be converging to the same solution. Crank-Nicolson (CN) timestepping is also examined and the results are given in Table 8.5.

Table 8.4 shows a first order convergence rate (fully implicit timestepping), while Table 8.5 shows a second order rate (CN timestepping). The results with CN timestepping also appear to be converging to the same solution.

N_S, N_{MD}	Timesteps	Value	Change	Ratio
35,20	60	15.9125	-	-
70,40	120	16.0586	0.1460	-
140,80	240	16.1138	0.0551	2.65
280,160	480	16.1386	0.0248	2.22
560,320	960	16.1500	0.0114	2.18
1120,640	1920	16.1554	0.0054	2.09

Table 8.4: Fully-Implicit timestepping results for the discretely observed maximum drawdown using similarity reduction under no-jumps. *MD-scaled* grids and linear interpolation are used. The model parameters are given in Table 8.1.

N_S, N_{MD}	Timesteps	Value	Change	Ratio
35,20	60	16.0517	-	-
70,40	120	16.1350	0.0833	-
140,80	240	16.1536	0.0186	4.49
280,160	480	16.1589	0.0053	3.49
560,320	960	16.1602	0.0013	4.07
1120,640	1920	16.1605	0.0003	3.92

Table 8.5: Crank-Nicolson timestepping is examined for the *MD* option using similarity reduction under Black-Scholes without jumps. *MD-scaled* grids and linear interpolation are used and parameters are given in Table 8.1. Convergence is approximately second-order.

Parameter	Value
S_0	100
T	1.0
σ	0.19
r	0.04
λ	0

Table 8.6: Parameters used for continuously observed Black-Scholes model for comparison with Pospisil *et al.*

N_S, N_{MD}	$N = N_{obs}$	Value	Change	Ratio
35,20	20	16.5941	-	-
70,40	80	19.2355	2.6414	-
140,80	320	20.5546	1.3191	2.00
280,160	1280	21.2165	0.6619	1.99
Extrapolated		21.8784		

Table 8.7: Fully-implicit timestepping is examined for the maximum drawdown option using similarity reduction under Black-Scholes without jumps. Convergence to the continuously observed case is examined. *MD-scaled* grids and linear interpolation are used and parameters are given in Table 8.6 The last row shows the extrapolated value assuming a consistent rate of convergence.

8.4 Comparison with Previous Work

The maximum drawdown option has been previously studied by Pospisil and Vecer for the continuously observed case without jumps[15]. By setting $N_{obs} = N$, where N is the number of timesteps and N_{obs} is the number of observation dates, we can converge to the continuously observed case by letting $N_{obs} \to \infty$, as the grid is refined. The values in Table 8.7 appear to agree with the graphical solution in [15]. However, convergence to the continuously observed limit is rather slow, as in the case of lookback options [28]. As in [28] for the lookback, we observe approximately square root convergence in terms of N_{obs} and as a result we increase the number of observations by a factor of four in each row of Table 8.7.

8.5 Validation with Monte Carlo

Parameter	Value
S_0	100
σ	0.095
r	0.04
λ	0.77
γ	0.094
μ_J	-0.149

Table 8.8: Parameters used for full jump-diffusion model [1].

N_S, N_{MD}	N	Value	Change	Ratio
35,20	60	13.3382	-	-
70,40	120	13.1909	-0.1473	-
140,80	240	13.1206	-0.0703	2.10
280,160	480	13.0986	-0.022	3.20
560,320	960	13.0921	-0.0065	3.38

Table 8.9: PIDE results for the discretely observed maximum drawdown option under jump-diffusion, using the parameters in Table 8.8 with $K = 0$, $T = 1.5$ and $N_{\text{obs}} = 5$. Crank-Nicolson timestepping is used.

We price the discretely observed maximum drawdown option with $K = 0$ under jump-diffusion using the parameters in Table 8.8 with $T = 1.5$ and $N_{\text{obs}} = 5$. These results are shown in Table 8.9.

For validation of our algorithm and these results, we compare the values in Table 8.9 with Monte Carlo (MC) simulation with jump-diffusion for the maximum-drawdown option with $K = 0$ and the same parameters in Table 8.8. We use forward Euler timestepping with M simulations, each having N timesteps. The MC results are given in Table 8.10, where we give the 95% confidence interval for the MC estimate. As expected, the PIDE solution appears to be converging to the same value as the MC estimate.

M (millions)	N	MC Value	95% Confidence
5	60	13.0251	0.0105
5	120	13.0556	0.0106
5	240	13.0701	0.0106
10	480	13.0842	0.0075
10	960	13.0842	0.0075

Table 8.10: Monte Carlo (MC) results for the discretely observed maximum drawdown option under jump-diffusion, using the parameters in Table 8.8 with $K = 0$. The 95% confidence interval is given on the MC estimate. M is the number of MC simulations, and N is the number of timesteps.

Chapter 9

Maximum Relative Drawdown Results

Here we show numerical results for the maximum relative drawdown option problem, where we demonstrate the advantage of the similarity reduction for arbitrary strike. We also test the jump model against a Monte Carlo simulation, and provide a possible rationalization for mutual fund fees.

9.1 Grid Type

We repeat the investigation done for the maximum drawdown case in Section 8.1 for the maximum relative drawdown without jumps using the data in Table 8.1. Table 9.1 indicates that the best convergence is obtained by using *MRD-scaled* grids with linear interpolation, which has a significant advantage over the *repeated* grid despite the inherent increase in interpolation error. As in Section 8.2, we ensure that the numerical localization error introduced by $M_{\min}$, $M_{\max}$, and $S_{\max}$ is insignificant compared to the discretization error. Specifically, we observe no change to six significant digits when increasing $M_{\max}$ and $S_{\max}$ by a factor of ten, and decreasing $M_{\min}$ by a factor of 10.

9.2 Strike

Although the maximum drawdown option with arbitrary strike K does not satisfy a similarity reduction, the maximum relative drawdown is homogeneous of degree zero (as seen in Equation 6.13), hence this permits similarity reduction. As a result, we investigate the convergence for the maximum relative drawdown with parameters given in Table 8.1, with in addition $K = 0.15$. Comparing

N_S, N_{MD}	N	Scaled (diagonal interp)	Scaled (linear interp)	Repeated
35,18	60	0.146847	0.147339	0.141638
70,36	120	0.147794	0.147963	0.146480
140,72	240	0.148068	0.148113	0.147725
280,144	480	0.148149	0.148164	0.148074
560,288	960	0.148175	0.148180	0.148158

Table 9.1: Comparison of grid type and interpolation methods for the maximum relative drawdown under Black-Scholes without jumps. The parameters used are in Table 8.1. As for the maximum drawdown, faster convergence is obtained when using both scaled grids and linear interpolation.

N_S, N_{MD}	N	Scaled (strike node)	Ratio	Scaled (no strike node)	Ratio
35,18	40	0.041578	-	0.041740	-
70,36	80	0.041832	-	0.041941	-
140,72	160	0.041886	4.67	0.041906	-5.75
280,144	320	0.041908	2.51	0.041914	-4.36
560,288	640	0.041914	3.22	0.041916	4.10
1120,576	1280	0.041916	3.38	0.041917	2.01

Table 9.2: Results for the maximum relative drawdown with strike $K = 0.15$ under Black-Scholes without jumps using a scaled grid with linear interpolation. The parameters used are in Table 8.1. When the strike node is removed from the scaled grid ($S = (1-K)S_0$) we observe erratic convergence.

Table 9.2 and 9.3, the convergence of the *MRD-scaled* grid is superior to the *repeated* grid. Note that if the node at the strike ($S = (1-K)S_0$) is removed, the convergence is somewhat erratic for the *MRD-scaled* grid as shown in Table 9.2. This behaviour is well documented in the literature and is due to the non-smoothness of the payoff at the strike [29].

9.3 Comparison of Jump-Diffusion to GBM

We now obtain the value of a maximum relative drawdown option under jump-diffusion with arbitrary strike K. The values are obtained using the parameters of

N_S, N_{MD}	N	Repeated	Ratio
35,18	40	0.037965	-
70,36	80	0.040888	-
140,72	160	0.041627	3.96
280,144	320	0.041850	3.31
560,288	640	0.041900	4.50
1120,576	1280	0.041913	3.78

Table 9.3: Results for the maximum relative drawdown with strike $K = 0.15$ under Black-Scholes without jumps using a repeated grid with linear interpolation. The parameters used are in Table 8.1.

$\sigma^I_{\text{NJ}}(T = 1)$	0.1765
$\sigma^I_{\text{NJ}}(T = 1.5)$	0.1780
$\sigma^I_{\text{NJ}}(T = 5)$	0.1796

Table 9.4: Implied volatility solved from Equation (9.1) for the given expiration time T and parameters used in Table 8.8.

Table 8.8. The plot in Figure 9.2 shows the *MRD* value plotted against the strike, K, with values accurate to three decimal places.

We determine the implied volatility σ^I_{NJ} for the no jump model ($\lambda = 0$) by solving,

$$V(\sigma^I_{\text{NJ}}, r, T, \lambda = 0, \gamma = 0, \mu_J = 0, S_0, \tau = 0) = V(\sigma, r, T, \lambda, \gamma, \mu_J, S_0, \tau = 0), \quad (9.1)$$

with a European call payoff, where $\{r, T, \lambda, \sigma_J, \gamma, \mu_J, S_0\}$ are given in Table 8.8.

Given the value for σ^I_{NJ}, which is given in Table 9.4, we compare the value of a maximum relative drawdown option under jump-diffusion to that of the no-jump case using the implied volatility for the given T, $\sigma^I_{\text{NJ}}(T)$. Figures 9.1 and 9.2 show the value of each case against the strike, K for $T = 1$ and $T = 5$, respectively.

With no strike ($K = 0$) the option under the jump-diffusion model is cheaper compared to the Black-Scholes. On the other hand, for larger strike values, the situation is reversed, and the option is more expensive when priced under jump-diffusion. The latter effect can be explained intuitively since the jumps in our case are generally large, which increases the probability of large drawdowns significantly. The changeover at lower strike is due to the significantly higher implied volatility for the no-jump model, which increases the likelihood of small drawdowns. This is illustrated in Figures 9.3 and 9.4, where we simulated ten

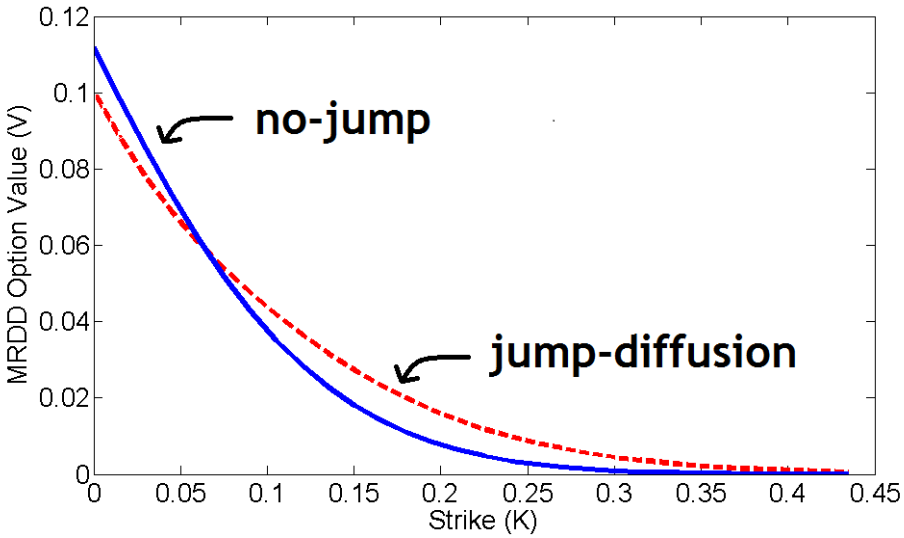

Figure 9.1: Values for *MRD* options with expiry time $T = 1$ as a function of the strike, K are compared for both jump-diffusion and a no-jump model with implied volatility calculated from Equation (9.1). Parameters are given in Table 8.8 where $N_{\text{obs}} = 5T$. Values are accurate to three decimal places.

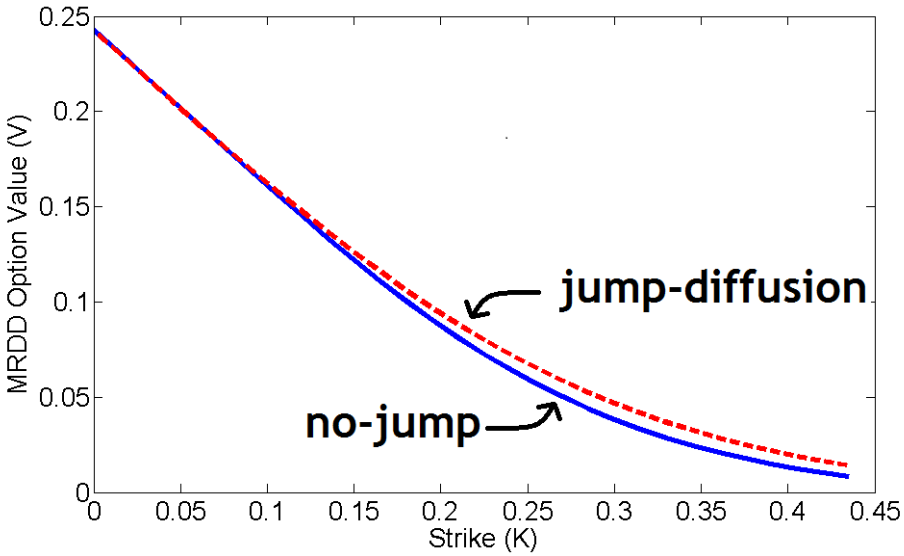

Figure 9.2: Values for *MRD* options with expiry time $T = 5$ as a function of the strike, K are compared for both jump-diffusion and a no-jump model with implied volatility calculated from Equation (9.1). Parameters are given in Table 8.8 where $N_{\text{obs}} = 5T$. Values are accurate to three decimal places.

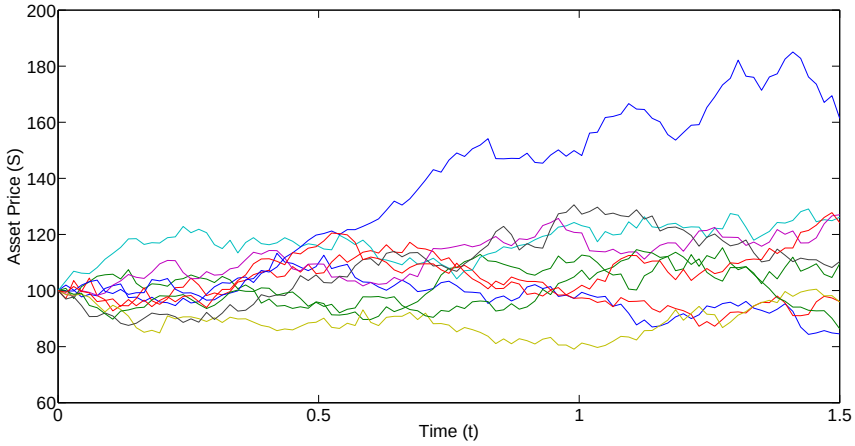

Figure 9.3: Monte Carlo simulation under jump-diffusion using parameters given in Table 8.8. The no jump model has higher average drawdown than the jump model shown in Figure 9.4.

Monte Carlo paths of the implied volatility under the no-jump case, and the jump-diffusion case. It is evident that significantly larger drawdowns can occur under jump-diffusion, with low probability, while smaller, more moderate drawdowns occur with the larger implied volatility (no-jump case) with high probability.

9.4 Application to Mutual Fund Fees

As discussed in Chapter 1, buying a maximum drawdown or maximum relative drawdown option can be viewed as a rationalization for mutual fund fees. Following the idea suggested by Guercio *et al.* *[14]* that investors are paying such fees for a service they value, which is unrelated to performance, investors may believe that the fund manager protects them from large drawdowns, effectively providing them with a drawdown option. Following this logic, assuming the fund holder pays a proportional fee of fS, we show the equivalent strike K for which the maximum relative drawdown has the same value. The option value is then given by,

$$V_\tau = \mathcal{L}_f V + \lambda \mathcal{J} V - fS, \tag{9.2}$$

where $\mathcal{L}_f V = \mathcal{L}V - fSV_S$ and the modifications to Eq. (3.3) account for the continuous proportional fee as described in [30]. Note that Equation (9.2) is no

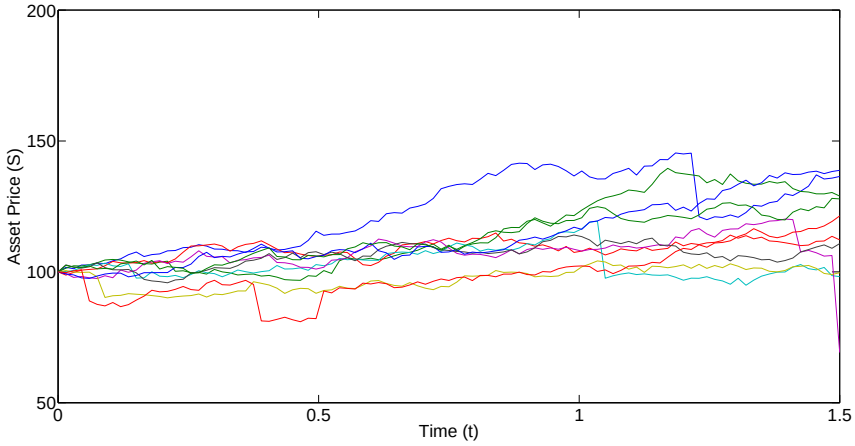

Figure 9.4: Monte Carlo simulation under jump-diffusion using parameters given in Table 8.8. The jump-diffusion model has much larger drawdowns (which occur less frequently) than the no-jump model in Figure 9.3.

T	1	2	5	10
K	16	18	19	15

Table 9.5: Equivalent strike K for which the maximum relative drawdown has price equal to the mutual fund fee of 3% per year. The parameters used for the option are given in Table 8.8, with modified expiry time T.

longer homogeneous of degree 0, and the similarity reduction does not hold for the maximum relative drawdown. In particular, Table 9.5 shows these results for a fee of $f = 3\%$.

As the length of the contract increases the equivalent option first tends to provide less protection (higher strike). This is somewhat intuitive; if you buy two separate one year options you can expect this to be cheaper than a two year option since the maximum drawdown will be at least as large as both one year drawdowns. On the other hand, as the time to maturity increases even further (above 5 years in Table 9.5), we see the discounted value of the fee becomes sufficiently large that it offsets this effect and the equivalent option provides more protection.

Table 9.5 indicates that a fee of about 3% per year would provide maximum relative drawdown insurance for any drawdowns larger than $15-20\%$. In other words, a possible explanation of why Canadian mutual fund fees are so high is that investors believe that active fund management protects them against large drawdowns.

Chapter 10

Conclusion

The maximum drawdown has been proposed as an ideal risk measure for capturing downside risk and is widely used in practice. Furthermore, investors are often drawdown averse and want to avoid large drawdowns. Although numerical methods exist for pricing continuous drawdowns under geometric Brownian motion [15], this does not solve the discretely observed problem under jump-diffusion.

In this thesis we developed a formulation to price both maximum drawdown options and maximum relative drawdown options. We extend the work of [15] using the general path-dependent formulation in [18]. We solve a set of one-dimensional problems under jump-diffusion for each discretized M and MD node, updating at discrete observation dates. In addition, we show that a similarity reduction can reduce the overall three-dimensional problem to two dimensions.

The key contributions of this thesis are:

- As in the cliquet case [18], scaled grids improve convergence over simple repeated grids by increasing node density near the update diagonals.
- Unlike the cliquet, diagonal interpolation proves ineffective.
- The similarity reduction holds under constant volatility for the maximum drawdown option with $K = 0$.
- Under constant volatility, the similarity reduction holds for the maximum relative drawdown option with arbitrary strike K.

We compare the option values with and without jumps, and show that the price is significantly different depending on the strike K. This demonstrates the importance of choosing an appropriate model for the valuation. At low strike, the no-jump option becomes more expensive, since a higher implied volatility leads to more moderate drawdowns. On the other hand, at high strike, the option

priced under jump-diffusion becomes more expensive since infrequent jumps may still cause large drawdowns. This also demonstrates that a moderate strike can reduce the costs of protection against large drawdowns.

Lastly, we compare the price of the relative drawdown option with that of mutual fund fees. A fee of 3% is not uncommon in the Canadian mutual fund marketplace. Hence, a possible explanation for these high fees is that investors are under the impression that active fund management will provide protection against maximum drawdowns of 20% or more.

10.1 Future Work

Possible future work could continue in a variety of directions.

- An extension of the financial model including a stochastic volatility jump-diffusion (SVJD) model. This would be a combination of Equation 2.8 and Equation 2.10. Recent work in this area includes [31].
- A formal proof that the similarity reduction maintains the stability of the scheme without the modification in Section 7.4.2. Since it is observed to remain stable, it is suspected that such a proof exists.
- An application of the maximum drawdown to wind energy could be explored. Wind generation has been modelled stochastically [32], and the drawdown describes the remaining charge in a battery. This may give rise to a variety of interesting problems, from optimizing battery capacity, to setting a fair price on the stablishment of wind turbines.

Bibliography

The numbers at the end of each entry list pages where the reference was cited. In the electronic version, they are clickable links to the pages.

[1] K. Matsuda. *Levy option pricing models: Theory and application*. PhD thesis, City University of New York, 2006. xiii, 44

[2] C. Pedersen. Derivatives and downside risk. *Derivatives Use, Trading and Regulation*, 7(3):251–268, 2001. 1

[3] M. Magdon-Ismail, A.F. Atiya, A. Pratap, and Y. Abu-Mostafa. The maximum drawdown of the Brownian motion. In *Computational Intelligence for Financial Engineering, 2003. Proceedings. 2003 IEEE International Conference on*, pages 243–247. IEEE, 2003. 1

[4] M. Magdon-Ismail, A.F. Atiya, A. Pratap, and Y. Abu-Mostafa. An Analysis of the Maximum Drawdown Risk Measure. *Risk Magazine*, 17(10):99–102, 2004. 1, 2

[5] D. Harding, G. Nakou, A. Nejjar, et al. The Pros and Cons of Drawdown as a Statistical Measure of Risk for Investments. *AIMA Journal*, pages 16–17, 2003. 1

[6] F. Schuhmacher and M. Eling. Sufficient conditions for expected utility to imply drawdown-based performance rankings. *Journal of Banking & Finance*, 2011. 1

[7] C.R. Bacon. *Practical portfolio performance measurement and attribution*. Wiley, 2008. 1

[8] R.H. Thaler. The end of behavioral finance. *Financial Analysts Journal*, 55(6):12–17, 1999. 1

[9] R. Hastie and R.M. Dawes. *Rational choice in an uncertain world: The psychology of judgment and decision making*. Sage Publications, Inc, 2009. 1

[10] Avner Mandelman. Gain-to-pain ratio can help you pick a fund. *Globe and Mail*, Oct 2010. 1

[11] B.G. Malkiel. Returns from investing in equity mutual funds 1971 to 1991. *Journal of Finance*, 50(2):549–572, 1995. 2

[12] J. Gil-Bazo and P. Ruiz-Verdu. The relation between price and performance in the mutual fund industry. *The Journal of Finance*, 64(5):2153–2183, 2009. 2

[13] J. Gil-Bazo and P. Ruiz-Verdú. When cheaper is better: Fee determination in the market for equity mutual funds. *Journal of Economic Behavior & Organization*, 67(3-4):871–885, 2008. 2

[14] D. Del Guercio, J. Reuter, and P.A. Tkac. Broker Incentives and Mutual Fund Market Segmentation. *NBER Working Paper*, 2010. 2, 51

[15] L. Pospisil and J. Vecer. PDE methods for the maximum drawdown. *Journal of Computational Finance*, 12(2):59–76, 2008. 2, 3, 4, 43, 53

[16] L. Pospisil and J. Vecer. Portfolio sensitivity to changes in the maximum and the maximum drawdown. *Quantitative Finance*, 10(6):617–627, 2010. 2

[17] L. Pospisil and J. Vecer. Maximum Drawdown of a Jump-Diffusion Process and the Corresponding Partial Integro-Differential Equations. 2, 17

[18] H. Windcliff, P.A. Forsyth, and K.R. Vetzal. Numerical methods and volatility models for valuing cliquet options. *Applied Mathematical Finance*, 13(4):353–386, 2006. 2, 19, 33, 35, 39, 53

[19] K.R. Vetzal and P.A. Forsyth. Discrete Parisian and delayed barrier options: A general numerical approach. *Advances in Futures and Options Research*, 10:1–16, 1999. 2

[20] R. Zvan, P.A. Forsyth, and K.R. Vetzal. Discrete Asian barrier options. *Journal of Computational Finance*, 3(1):41–67, 1999. 2

[21] H. Windcliff, P.A. Forsyth, and K.R. Vetzal. Shout options: A framework for pricing contracts which can be modified by the investor. *Journal of Computational and Applied Mathematics*, 134(1-2):213–241, 2001. 2

[22] F. Black and M. Scholes. The pricing of options and corporate liabilities. *The journal of political economy*, 81(3):637–654, 1973. 11

[23] D. Tavella and C. Randall. *Pricing financial instruments: The finite difference method*. John Wiley & Sons, 2000. 19

[24] Y. d'Halluin, P.A. Forsyth, and K.R. Vetzal. Robust numerical methods for contingent claims under jump diffusion processes. *IMA Journal of Numerical Analysis*, 25(1):87, 2005. 28, 29, 30

[25] J. Wang and PA Forsyth. Maximal use of central differencing for hamilton-jacobi-bellman pdes in finance. *SIAM Journal on Numerical Analysis*, 46(1580-1601):1–60, 2008. 29

[26] G. Barles. Convergence of numerical schemes for degenerate parabolic equations arising in finance theory. *Numerical methods in finance*, 1997. 30

[27] M. Briani, C.L. Chioma, and R. Natalini. Convergence of numerical schemes for viscosity solutions to integro-differential degenerate parabolic problems arising in financial theory. *Numerische Mathematik*, 98(4):607–646, 2004. 30

[28] C.F. Cheuk Ton and H.F. Terry. Currency lookback options and observation frequency: a binomial approach. *Journal of International Money and Finance*, 16(2):173–187, 1997. 43

[29] D.M. Pooley, K.R. Vetzal, and P.A. Forsyth. Convergence remedies for non-smooth payoffs in option pricing. *Journal of Computational Finance*, 6(4):25–40, 2003. 48

[30] H. Windcliff, P.A. Forsyth, and K.R. Vetzal. Valuation of segregated funds: shout options with maturity extensions. *Insurance: Mathematics and Economics*, 29(1):1–21, 2001. 51

[31] G. Yan and F.B. Hanson. Option pricing for a stochastic-volatility jump-diffusion model with log-uniform jump-amplitudes. In *American Control Conference, 2006*, pages 6–pp. IEEE, 2006. 54

[32] P. Pinson, L.E.A. Christensen, H. Madsen, P.E. Sørensen, M.H. Donovan, and L.E. Jensen. Regime-switching modelling of the fluctuations of offshore wind generation. *Journal of Wind Engineering and Industrial Aerodynamics*, 96(12):2327–2347, 2008. 54